

Determination of cloud liquid water distribution using 3D cloud tomography

Dong Huang,¹ Yangang Liu,¹ and Warren Wiscombe^{1,2}

Received 5 July 2007; revised 12 February 2008; accepted 26 February 2008; published 2 July 2008.

[1] The cloud microwave tomography method for remotely retrieving 3D distributions of cloud Liquid Water Content (LWC) was originally proposed by Warner et al. in the 1980s but has lain dormant since then. This paper revisits and extends the cloud tomography method by rigorously examining the nature of the resultant mathematical problem and its close relationship to the physical configuration of microwave radiometers. The singular value decomposition (SVD) analysis reveals that the retrieval of cloud LWC fields from microwave emission is highly ill-posed, and requires special techniques to solve it. The truncated SVD approach along with the L-curve method for choosing the optimal truncating point is used to obtain a better retrieval of cloud LWC. A group of sensitivity studies show that the retrieval accuracy is determined by several factors, including the number of radiometers, the spatial resolution of output, the number of scanning angles, the radiometer characteristics (e.g., noise level, beam width), the physical arrangement of radiometers, and the uncertainty in the ancillary temperature and water vapor mixing ratio data. When more radiometers and/or more scanning angles are used, and/or the radiometer beam width is reduced, and/or when a coarser output resolution is acceptable, the retrieval problem becomes less ill-posed, and a better retrieval can be obtained. Moreover, the observation system simulations demonstrate that the cloud tomography method is able to retrieve the cloud structures generated by cloud resolving models with a good accuracy. For a setup consisting of four microwave radiometers of typical noise level 0.3 K, the tomography method is capable of retrieving the LWC to within 5% of the maximum LWC in the simulated stratocumulus and broken cumulus cases, with a spatial resolution of a few hundred meters.

Citation: Huang, D., Y. Liu, and W. Wiscombe (2008), Determination of cloud liquid water distribution using 3D cloud tomography, *J. Geophys. Res.*, 113, D13201, doi:10.1029/2007JD009133.

1. Introduction

[2] Clouds in the lower troposphere are an important component of the hydrologic cycle, and also exert enormous influences on the Earth's radiation budget. Consistent observations of clouds are needed in many relevant areas such as weather forecasting and climate modeling, and have received a lot of attention in the past several decades. For example, the overarching goal of the Atmospheric Radiation Measurement (ARM) program is to improve this representation of cloud and radiation in climate models, partly by providing long-term consistent data products [Ackerman and Stokes, 2003]. For more than 10 years, ARM has been collecting data related to radiation and clouds at three primary sites representing a wide range of climatic conditions. Despite the great efforts, spatial distribution of cloud water, a key aspect of clouds, is still one of the

largest uncertainties in global climate models [Stephens, 2005]. Part of the reason is that existing techniques don't provide a full view of clouds: they either sample a small volume of a cloud or measure only the vertical integral of the Liquid Water Content (LWC). For example, in situ measurements employ hot wires or optical probes on an aircraft to determine cloud LWC. The sample volume of such techniques is so small that it would take thousands of years to measure an entire cloud [Wiscombe, 2005]. On the other hand, active remote sensing techniques like cloud radar [Hogan et al., 2005] with rapid scanning capability seem promising, but they provide a less direct measurement of cloud water content (since radar reflectivity depends strongly on the particle size distribution) and also would likely be much more costly than passive methods.

[3] Single microwave radiometers have been widely used in passive remote sensing to measure cloud liquid water and water vapor [Westwater et al., 2004]. They mainly provide path-integrated amounts since they have poor resolution along the measurement path. To improve on their spatial resolution, microwave tomography methods were proposed by Warner et al. [1985, 1986], Warner and Drake [1988], Twomey [1987], and Drake and Warner [1988]. Tomogra-

¹Environmental Sciences Department, Brookhaven National Laboratory, Upton, New York, USA.

²NASA Goddard Space Flight Center, Code 913, Greenbelt, Maryland, USA.



Figure 1. Comparison of a scanning microwave radiometer made more than 25 years ago (left [Snider *et al.*, 1980; Hogg *et al.*, 1983]), used by Warner *et al.* [1986] in a cloud tomography demonstration, with a recently developed Ground-based Scanning Radiometer (right, [Cimini *et al.*, 2007]) deployed in Barrow, Alaska, USA during 2004. The Snider radiometer operates at two frequencies (23.8 and 31.4 GHz). The scanning bearings are on the top of the trailer; the electronics and antenna are located in the trailer to keep a benign working environment. Ground-based Scanning Radiometer (GSR) is a multi-frequency scanning radiometer operating from 50 to 380 GHz; it can provide unprecedented information on the evolution of temperature, water vapor, and clouds. The photo shows that the scanhead moved out of the framework for atmospheric viewing. The circles are the radiometers of different wavelengths mounted on the scanhead.

phy has been widely used in different disciplines such as medical imaging, archaeology, biology, geology, astronomy, and oceanography. Perhaps one of the most famous applications is the X-ray transmission computed tomography used for imaging the internals of a human body. Tomography is also found useful in imaging the Earth's atmosphere: Fleming [1982] and Hoffman *et al.* [1989] simulated retrieving cross sections of the vertical atmospheric temperature structure from satellite radiance measurements taken at various angles and frequencies; Flores *et al.* [2000] retrieved the tropospheric water vapor distribution using the wet delay data derived from a locally dense network of GPS receivers.

[4] Warner *et al.* [1985, 1986] pioneered cloud tomography using two microwave radiometers to determine the spatial distribution of cloud LWC. Their setup involved planar-scanning a cloud with two ground-based microwave radiometers, although, in six weeks of scanning, only one cloud passed between the two radiometers that could yield a credible tomographic retrieval. Their retrieval algorithm, nonnegative least squares, was that of Lawson and Hanson [1974]. The simulation studies demonstrated that cloud tomography was capable of estimating LWC to within 10% of the maximum LWC with a spatial resolution of a few hundred meters. Twomey [1987] developed an iterative nonlinear inversion algorithm for tomographic problems to reduce the computation cost, which was a major limit at that time. Drake and Warner [1988] performed computer simulations of tomographic retrieval of cloud LWC with an airborne radiometer, and their retrieval algorithm was similar to that of Warner *et al.* [1985]. A field test of this setup was carried out in Louisiana and the LWC deduced from the radiometric measurements showed statistically good agreement with that measured directly by an airborne Particle Measurement System [Warner and Drake, 1988].

[5] Unfortunately, the cloud tomography subject has lain dormant since the pioneering works, leaving some impor-

tant questions unanswered. For example, the mathematical nature of the cloud tomography retrieval problem and its relationship to the physical configuration has not been rigorously examined, although they are essential not only for optimizing the retrieval algorithm but also for determining the best physical arrangement of radiometers and the optimal scanning strategy. In the intervening 20 years, many advances have been made in the relevant areas (e.g., smaller, cheaper and more efficient microwave radiometer technology; more realistic 3D cloud-resolving models; better mathematical methods for ill-posed problems; and faster computer speed), permitting a better investigation of the cloud tomography technique. For example, Figure 1 shows the evolution of the 1980-generation dual-frequency radiometers used by Warner *et al.* [1986] to the contemporary multifrequency ground-based scanning radiometer. Not only have the radiometers become much more mobile, but also the calibration technique has been advanced from the tipping curve calibration [Snider *et al.*, 1980; Hogg *et al.*, 1983] to the more accurate calibration method using two external blackbody references [Cimini *et al.*, 2007]. Together with the need for measuring 3D distributions of cloud LWC, a renaissance of the cloud tomography is now timely.

[6] In this paper, we revisit the cloud tomography technique, and discuss several improvements on the tomography setup of Warner *et al.* [1985]. We also examine the mathematical nature of the retrieval problem, specifically its ill-posedness, and demonstrate the usefulness of combining the truncated singular value decomposition (SVD) method [Hansen, 1990] and the L-curve method [Hansen, 1992] to obtain better retrievals. The paper is organized as follows. Section 2 provides a description of the theoretical formulation of the cloud tomography method. Section 3 elaborates the mathematical nature of the tomographic retrieval problem. Section 4 shows some observing system simulations of cloud tomography including sensitivity studies. A summary

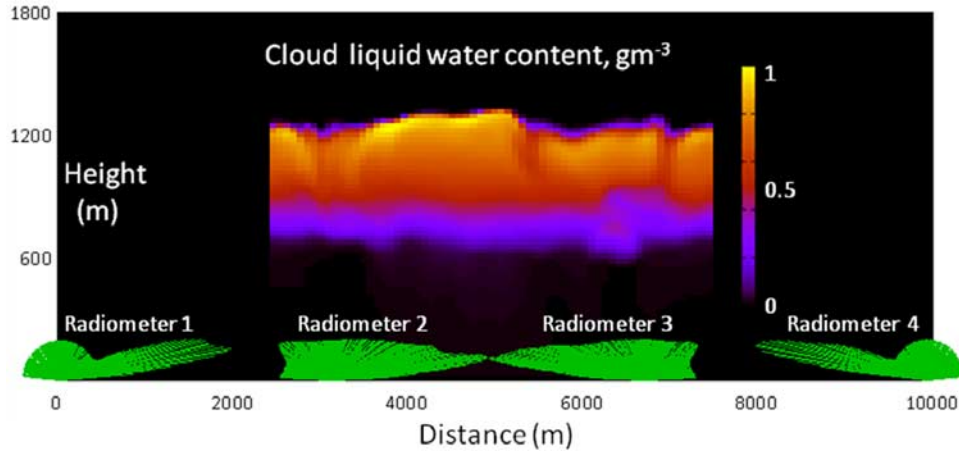


Figure 2. Illustration of the working principle of a four-radiometer ground-based cloud tomography setup. The stratocumulus cloud is a two-dimensional 5-km wide by 1.5-km high slice taken from a large eddy simulation model. Four scanning radiometers spaced 3.3 km apart with 0.3 K noise level are arranged in a line 10 km long. Each radiometer scans the upper plane to within 5° of the ground; the scans are every 2.0° in angle, giving a total of 200 rays from the four radiometers hitting the cloudy area. The lengths of the scan lines from each radiometer are proportional to the simulated brightness temperatures in that direction. The atmospheric background is assumed to be 20 K.

of the findings in this study and discussions on improving and extending cloud tomography are given in section 5.

2. Observing System Simulation for Cloud Tomography

[7] Observing System Simulation Experiment (OSSE) is a useful tool to study a forecast or retrieval system. The OSSE for cloud tomography mainly contains two components: a forward model to generate the atmospheric state and simulate the microwave measurements, and an inverse algorithm to retrieve the cloud water field from the simulated microwave data. Specifically, the forward model first generates the atmosphere state variables using a cloud resolving model (section 4), then computes the microwave measurements using the radiative transfer equation. Figure 2 shows an example of a four-radiometer tomography setup measuring a stratocumulus cloud.

[8] The radiative transfer equation relating the microwave radiation intensity to the atmosphere state is:

$$I(\Omega_i) = I_\infty \tau(\Omega_i, 0, \infty) + \int_0^\infty B(T) \alpha(s, \Omega_i) \tau(\Omega_i, 0, s) ds, \quad (1)$$

where $I(\Omega_i)$ is the intensity of radiation reaching a radiometer from direction Ω_i ; I_∞ is the intensity of the cosmic background radiation; $B(T)$ is the Planck function at temperature T ; α is the absorption coefficient determined by the atmosphere state; and $\tau(\Omega_i, s_1, s_2) = \exp[-\int_{s_1}^{s_2} \alpha(s, \Omega_i) ds]$ is the transmission between two points s_1 and s_2 along direction Ω_i . Since transmission decreases along photon path, emission signal from clouds far from the radiometer is likely to be severely attenuated by the atmosphere. Therefore we restrict cloud tomography to map the cloud structure over a field of 5 km wide and 1.5 km high. Furthermore, very large zenith angles ($>85^\circ$) are excluded in our simulations to avoid very long photon path in the low troposphere,

significant atmospheric refraction, and side lobe contributions from ground clutters.

[9] For ice-free clouds (ice would add the complication of scattering), cloud tomography measures the line integrals of cloud emission along many directions. These integrals are related to the spatial distribution of cloud absorption coefficients by the microwave radiative transfer equation (equation (1)) and are measured by the microwave radiometers. A radiometer measurement \bar{I} is the convolution of I with the antenna gain pattern G , which in this study is assumed to decrease exponentially with the square of angular departure from the center axis Ω_i [Drake and Warner, 1988],

$$\begin{aligned} \bar{I}(\Omega_i) &= \int I(\Omega) G(\Omega - \Omega_i) d\Omega, \\ G(\xi) &= \frac{1}{w} \left(\frac{4 \ln 2}{\pi} \right)^{1/2} \exp \left[-4 \ln 2 \left(\frac{\xi}{w} \right)^2 \right]. \end{aligned} \quad (2)$$

Here w stands for the width of the antenna beam between rays where the gain is half its maximum value.

[10] Substituting equation (1) into equation (2), taking into account the equality $\tau(\Omega_i, s_1, s_2) = \tau(\Omega_i, s_1, s) \tau(\Omega_i, s, s_2)$, and approximating the angular integral using the Gauss quadratures, we get:

$$\begin{aligned} & \sum_{k=1}^{N_H} w_k \tau(\Omega_{ik}, 0, s_1) \int_{s_1}^{s_2} B \alpha \tau(\Omega_{ik}, s_1, s) ds \\ &= \bar{I}(\Omega_i) - \sum_{k=1}^{N_H} w_k I_\infty \tau(\Omega_{ik}, 0, \infty) - \sum_{k=1}^{N_H} w_k \\ & \quad \times \left[\int_0^{s_1} B \alpha \tau(\Omega_{ik}, 0, s) ds + \tau(\Omega_{ik}, 0, s_2) \int_{s_2}^\infty B \alpha \tau(\Omega_{ik}, s_2, s) ds \right] \end{aligned} \quad (3)$$

Here N_H is the number of the Gauss quadratures; w_k is the weight of the antenna gain pattern corresponding to the

Gauss quadratures; s_1 and s_2 are the path lengths from the radiometer to the locations at which the ray with direction Ω_i enters and leaves the cloud.

[11] Given a total number of m rays, equation (3) can be further discretized by dividing a field, which is large enough to contain the cloud, into $n = N^3$ (N^2 for a 2D slice) equal size volume pixels to yield the following matrix equation:

$$\mathbf{Ax} = \mathbf{b}, \quad (4)$$

where $\mathbf{x}^T = (\alpha_1, \alpha_2, \dots, \alpha_n)$ is the vector of absorption coefficients; $\mathbf{b}^T = (b_1, b_2, \dots, b_m)$, is the vector of measurements, b_i equals the right side of equation (3); and $\mathbf{A} = (\alpha_{ij})$ is an $m \times n$ matrix with

$$a_{ij} = \sum_{k=1}^{N_H} w_k \tau(\Omega_{ik}, 0, s_1) \int_{s_1}^{s_2} B \varphi_j(s, \Omega_{ik}) \tau(\Omega_{ik}, s_1, s) ds. \quad (5)$$

$\varphi_j(s, \Omega_{ik})$ is nonzero only if the point (s, Ω_{ik}) is in the j th cloud pixel, and there $\varphi_j = 1$. When cloud is found in the retrieval to occupy only part of the field or the information of cloud boundary is available from other measurements like Radar, the retrieval process can be refined with a smaller field to get a better spatial resolution.

[12] The dependence of the microwave measurements on these atmospheric state variables is introduced by the absorption coefficient (equations (1), (3), and (4)). In clouds, the absorption coefficient consists generally of contributions from liquid water (α_l), water vapor (α_v), and molecular oxygen (α_{O_2}). The formulae for calculating absorption coefficient for nonprecipitating clouds, given state variables of the atmosphere, are those of *Westwater* [1972] and *Falcone* [1966]; they are also specified in the Appendix of *Warner et al.* [1985]. The absorption coefficient is simply a linear function of LWC,

$$\alpha = \kappa_l \cdot LWC + \alpha_v + \alpha_{O_2}, \quad (6)$$

where κ_l is the absorption efficiency of liquid water and depends only on temperature, and wavelength. The radiometric characteristics of the three absorptive agents underlie the criteria for choosing the appropriate working frequency in cloud tomography, that is, a moderate emission strength of liquid water, and a weak absorption of water vapor and oxygen [Warner et al., 1985]. At the frequency of 31.6 GHz (about 1.0 centimeter in wavelength), the absorption efficiencies of water vapor and oxygen are usually two and four orders less in magnitude than that of liquid water at typical atmospheric conditions. For example, the absorption efficiencies of liquid water, water vapor, and oxygen are $1.5 \cdot 10^{-4}$, $1.1 \cdot 10^{-6}$, and $1.6 \cdot 10^{-8} \text{ m}^{-1} (\text{gm}^{-3})^{-1}$ at the one kilometer altitude in a U.S. Standard Atmosphere 1976 (temperature 281.7 K, pressure 89875 Pa). So the requirement for the accuracy of water vapor and oxygen to be known is not high in cloud tomography. Nevertheless, the relative contributions of these absorptive agents also depend on their relative concentrations in the atmosphere. It might be difficult for cloud tomography to resolve a small amount of liquid water in a very moist environment.

[13] It is necessary to know atmospheric temperature, pressure, and water vapor mixing ratio, e.g., from a radio-

sonde, to be able to retrieve cloud liquid water distribution by inversion procedures. With this, the first step in the retrieval of LWC is to solve equation (4) for the vector \mathbf{x} of absorption coefficients, given the vector \mathbf{b} of scanning microwave data. Then LWC can be easily deduced from equation (6). The transmission terms in equations (3) and (4) are related to absorption coefficients, thus the inversion is actually nonlinear. In practice, an iterative method is used to build the converged retrieval: an estimate of absorption coefficient α within the cloud is first made from the scanning data with the cloud taken to be homogeneous, and it is used to compute the matrix \mathbf{A} and solve equation (4) for a new set of cloud absorption coefficients. Successive substitutions are performed until the set of cloud absorption coefficients converge. The speed of convergence is determined by the linearity of equation (4), and fortunately it is very close to linear because the dependence of transmission terms in equation (3) on absorption coefficients is weak for nonprecipitating clouds.

3. Retrieval Method

[14] As will become clear later, the matrix \mathbf{A} in equation (4) has a large condition number, which indicates that the inverse problem is ill-posed (the solution is highly sensitive to any errors in measurements and/or matrix \mathbf{A}). For such a problem, an ideal, unambiguous retrieval would require the data and \mathbf{A} to be free of noise and each cloud element to be scanned from all directions [Davison, 1983; Olson, 1995]. Because both conditions are impossible to meet in reality, multiple solutions may satisfy the same radiometric measurements, and special regularization techniques beyond the standard method of least squares are needed to deal with this problem. Furthermore, determination of the optimal solution depends critically on the ill-posed nature of the inverse problem. However, the nature of the inverse problem and its relationship to the physical configuration of the radiometers have not been rigorously examined in previous studies. To fill this gap, this section first examines the ill-posedness of the cloud tomography, and then discusses the regularization technique to solve the corresponding inverse problem.

3.1. SVD Examination of the Ill-Posedness

[15] The $m \times n$ matrix \mathbf{A} ($m \geq n$) can be decomposed as:

$$\mathbf{A} = \mathbf{U} \Sigma \mathbf{V}^T = \sum_{i=1}^n u_i \sigma_i v_i^T. \quad (7)$$

Here $\mathbf{U} = (u_1, u_2, \dots, u_n)$ is an $m \times n$ orthogonal matrices containing a set of orthonormal input basis vector directions u_i for \mathbf{A} , and $\mathbf{V} = (v_1, v_2, \dots, v_n)$ is an $n \times n$ orthogonal matrices containing a set of output basis vector directions v_i for \mathbf{A} ; while $\Sigma = \text{diag}(\sigma_1, \sigma_2, \dots, \sigma_n)$ is an diagonal matrix with the nonnegative singular values ordered such that $\sigma_1 \geq \sigma_2 \geq \dots \geq \sigma_n \geq 0$. The condition number of matrix \mathbf{A} is defined as the ratio of the maximum to the minimum nonzero singular value, and its value characterizes the ill-posedness of the underlying problem [Hansen, 1998]. A bigger condition number means that the problem is more ill-posed, and the solution is more sensitive to measurement noises or numerical errors.

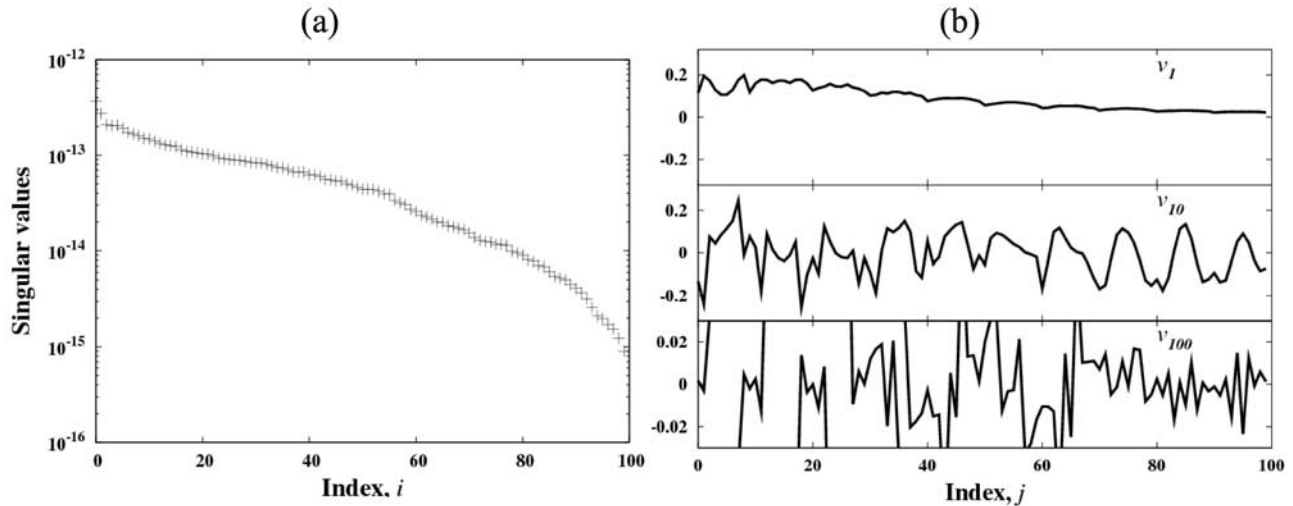


Figure 3. Singular value decomposition of the matrix \mathbf{A} for the tomographic retrieval problem described in section 3.1. (a) The singular values decay to almost zero as the index i increases. (b) The output vectors v_i have more sign changes in their elements as the index i increases. There are no sign changes in the first output vector v_1 , while there are 27 sign changes in v_{10} and 64 sign changes in the last output vector v_{100} .

[16] The least squares solution of equation (5) then can be written as:

$$\mathbf{x}_{\text{LS}} = \mathbf{V}\Sigma^+\mathbf{U}^T\mathbf{b} = \sum_{i=1}^n \frac{u_i^T \mathbf{b} v_i}{\sigma_i}, \quad (8)$$

where Σ^+ is the transpose of Σ with every nonzero element replaced by its reciprocal, and it equals the inverse of Σ when \mathbf{A} is square. equation (8) suggests that the least squares solution is a linear combination of the input and output vectors (u_i and v_i) weighted by the reciprocals of σ_i . Therefore the number of sign changes in the elements of the input and output vectors is another characteristic feature of ill-posed problems [Hansen, 1998].

[17] Consider as an example a stratocumulus cloud with a four-radiometer setup (Figure 2, a detailed description is also provided in section 4). Figure 3a shows the singular values of the corresponding matrix \mathbf{A} decay gradually to a very small value with no particular gap in the spectrum. In connection with ill-posed problems, the gradual decrease of the singular values is a characteristic feature of the ill-posedness [Hansen, 1998]. The condition number for this case is 420, which provides a quantitative measure of the ill-posedness of the problem. Figure 3b reveals that the output vectors v_i tend to have more sign changes in their elements as the index i increases: no sign changes in v_1 , 27 changes in v_{10} , and 64 changes in v_{100} . The same is also true for the input vectors u_i . These patterns of sign changes in the input and output vectors coincide with the characteristic features of the SVD of an ill-posed problem.

3.2. Truncated SVD and L-Curve Method

[18] The standard least squares method, which aims to find the solution that will minimize the difference between simulated and measured data, is widely used in the inversion of well-posed problems. For such an ill-posed problem as that of the cloud tomography, existence of small singular

values makes the solution derived from the standard method very sensitive to measurement noises and numerical errors, and as a result, the inevitable noises/errors make this solution unrealistic (see equation (8)). Furthermore, multiple solutions exist within the uncertainty of measurements (see next for the demonstration of these issues).

[19] A widely used method for solving these ill-posed problems is the so-called regularization. Among many regularization techniques, the truncated SVD method is easy to implement and provides a clear physical image on how does regularization reduce the retrieval sensitivity owing to ill-posing [Hansen, 1990]. Unlike the standard least squares method that is equivalent to keeping all the singular values, the truncated SVD method is to impose a smoothness constraint to the solution by discarding the highly oscillating parts associated with small singular values. By doing this, the sensitivity to noises and numerical errors of the problem is reduced. Of course, the truncated SVD method reduces to standard least squares method when no singular values are in fact truncated.

[20] The key to the truncated SVD method is to determine where to truncate the singular values. Too many truncated singular values mean that too much smoothness is imposed on the solution, whereas too few truncated singular values mean that the noises in measurements are magnified too much in the solution. The truncating point that gives the optimal retrieval is determined using the L-curve technique discussed by Hansen [1992]. The L-curve corresponding to the truncated SVD is a log-log plot of the 2-norm of the solution $\|\mathbf{x}\|^2$ versus the residual norm $\|\mathbf{A}\mathbf{x} - \mathbf{b}\|^2$ for all possible truncating parameters (the ‘‘truncating parameter’’ is defined as the percent of truncated singular values). As illustrated in Figure 4a, the 2-norm of the solution falls precipitously when the first few small singular values are truncated, while the residual norm remains almost unchanged. When more singular values are truncated, the 2-norm of the solution stops declining and the residual

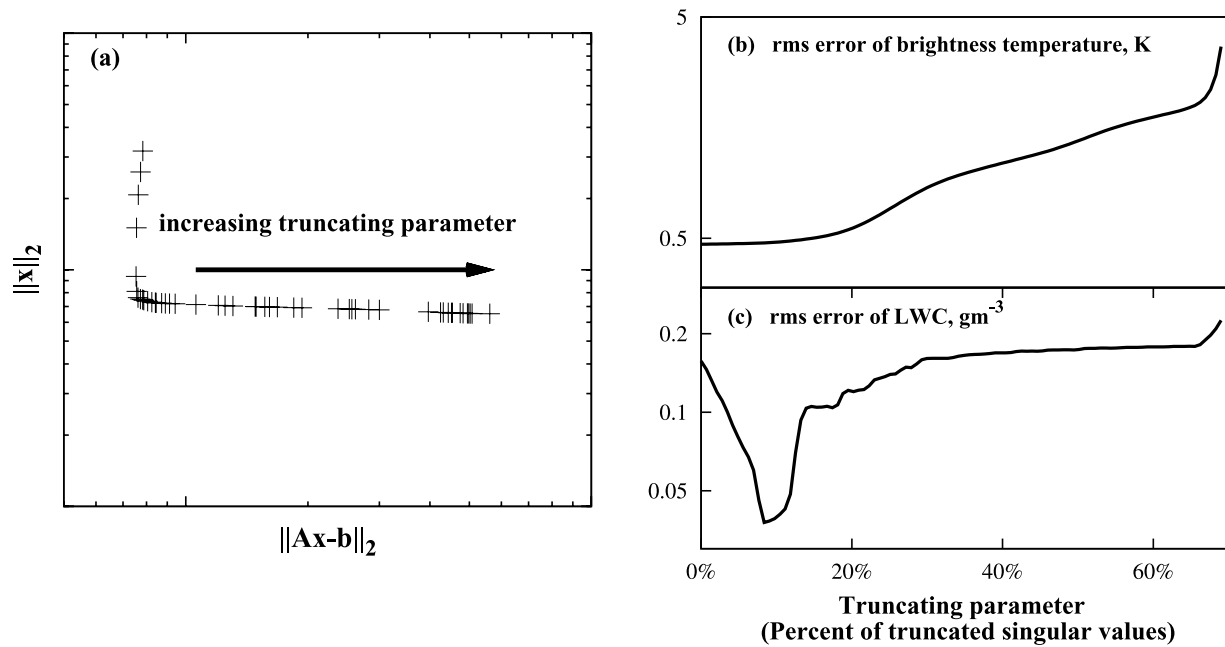


Figure 4. Illustration of obtaining optimal retrieval of LWC through the truncated SVD method. (a) Schematic illustration of the L-curve. The corner of the L-curve is usually not far from the point which gives the optimal retrieval. (b) The RMS error of microwave brightness temperature as a function of the truncating parameter, defined as percent of the singular values that are neglected in the retrieval algorithm. The standard least squares method corresponds to the case that the truncating parameter is zero. Figure 4c is the same as Figure 4b, but for the RMS error of the retrieved LWC. The RMS error of LWC from the standard least squares method is four times higher than that from the truncated SVD method.

norm starts to increase. The optimal truncating parameter usually corresponds to the sharp corner of the L-curve. Thus locating the L-curve's corner is paramount. In this work, we use an algorithm similar to that in Chapter 7 of Hansen [1998] to determine the corner but based on a numerically more stable criterion of minimum distance to the origin instead of the criterion of maximum curvature.

[21] Consider the same example as in section 3.1, we use the truncated SVD to calculate the solution of equation (4). The residual error of microwave radiance keeps increasing as more singular values are truncated (Figure 4b); with very slow increasing (almost flat in the logarithm scale) up to the 20% truncating point and rapid increasing after the 20% point. But the RMS error of LWC shows a very different behavior; it first declines, reaching a minimum around the 10% point, followed by a rapid increase (Figure 4c). The optimal retrieval of cloud LWC is not achieved at the point where the difference between simulated and measured microwave signals is minimized, although that is the point chosen by the standard least squares method. The standard least squares method thus yields a LWC error four times higher than that from the truncated SVD method. This discrepancy indicates that the retrieval is ill-posed, and the standard least squares method cannot produce the optimal retrieval.

4. Results

[22] The simulation experiments by Warner *et al.* [1985] were based on a simplified, onion-like cloud, which consists

of a “juicy” central core surrounded by rings of decreasing water content toward the cloud edge. Better experiments are possible now with the emerging of 3D cloud resolving models in the intervening 20 years and allow us to examine the capability of cloud tomography to retrieve more realistic spatial patterns of cloud water content. Also, with a rigorous examination of the mathematical nature of the retrieval problem (section 3), we are now able to investigate the utility of more advanced retrieval methods such as the truncated SVD method in cloud tomography. Furthermore, several key factors like the physical setup of radiometers and the spatial resolution of output were not discussed in the sensitivity studies of Warner *et al.* [1985], although they are critical for the tomographic retrieval accuracy. We have a close examination of such factors in this section, as such a task is certainly necessary to improve the physical design of cloud tomography.

[23] If not stated, the tomographic specifications in the simulations take the following default values (Figure 2): the total number of radiometers used is four, each with 0.3 K noise level and 2° beam width; the radiometers are placed linearly on the ground with the distance between the first and the last being 10 km; the resolution of output images is 10 by 10; the total number of rays intersecting the retrieval domain is two times of the total number of pixels; the water vapor mixing ratio is known from a radiosonde within a relative accuracy of 5% and the atmospheric temperature is accurate to within 1.0 K. The 2° beam width and 0.3 K noise level with 1-s integration time are representative of the state of the art of current microwave radiometers [Westwater

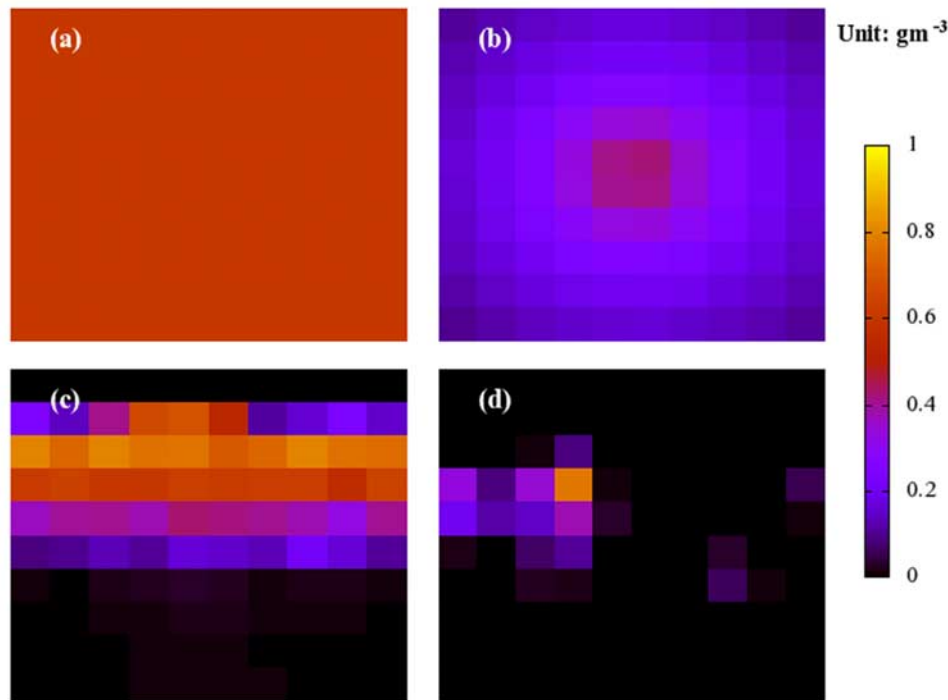


Figure 5. Liquid water fields of the following four cloud cases: (a) homogeneous cloud, (b) onion cloud, (c) stratocumulus cloud, and (d) broken cumulus cloud.

et al., 2004; *Mattioli et al.*, 2005]. The 200 scanning angles is approximately the number of “useful” scanning angles (those intersect with the retrieval domain) we can get with four radiometers of 1-s integration time in a 2-min period.

4.1. Examples of the Cloud LWC Retrieval

[24] For ease of comparison with *Warner et al.* [1985] and of visualization, here we only show the simulations using the 2D slices of the 3D cloud fields. The cloud tomography approach has been applied to the four cloud cases shown in Figure 5, for four tomography setups differing with each other in either the number of radiometers or the output resolution (see Table 1). Note that the original high resolution images (not shown here) are degraded to the desired output resolution before simulating the radiometer measurements, in order to minimize the possible impact of discretization which would complicate the interpretation of the sensitivity studies. The first cloud case is an ideally homo-

geneous cloud with a constant LWC. The second case is an onion-like cloud with a juicy core in the center, which is similar to the “onion” distribution used by *Warner et al.* [1985]. The third case is a stratocumulus cloud simulated by the DHARMA large eddy simulation model driven by data from Atlantic Stratus Experiment [*Ackerman et al.*, 1995]. The fourth case is also from the DHARMA model but is a patchy cumulus situation based on Atlantic Tradewind Experiment data. The maximum and mean LWC values of each cloud case range from 0.5 to 1 gm^{-3} and 0.03 to 0.6 gm^{-3} (Table 1), respectively. The cloud field in all cases is 5000 m wide and 1500 m high.

[25] We use relative error as a metric of retrieval quality to keep the same reference point as in *Warner et al.* [1985]. Relative retrieval error is computed as the ratio of the RMS error of LWC to the maximum LWC value within the cloud. The metric for the truncated SVD

Table 1. Relative Error of the LWC Retrieved by the Truncated SVD Method for Each of the Following Four Cloud Tomography Setups and Four Cloud Cases^a

Cloud Cases	Max LWC, gm^{-3}	Mean LWC, gm^{-3}	Relative Errors			
			Setup I 2 Radiometers 10×10 Pixels	Setup II 4 Radiometers 10×10 Pixels	Setup III 8 Radiometers 10×10 Pixels	Setup IV 8 Radiometers 20×20 Pixels
Homogeneous	0.60	0.60	12%(32%)	5%(17%)	3%(5%)	5%(28%)
Onion	0.50	0.20	13%(26%)	5%(15%)	3%(6%)	6%(24%)
Stratocumulus	0.97	0.23	14%(27%)	5%(11%)	3%(5%)	8%(22%)
Broken cumulus	1.0	0.03	7%(33%)	4%(8%)	3%(4%)	6%(21%)

^aThe tomography setups are different with each other in either number of radiometer or output resolution. The cloud fields are 5000 m wide and 1500 m high. Since the radiometer noise is a random function from ray to ray, the relative error metric is computed as the mean relative error from 10 runs for each combination of cloud case/setup. The values in the parenthesis correspond to the standard least squares method. The values in the parenthesis correspond to the standard least squares method.

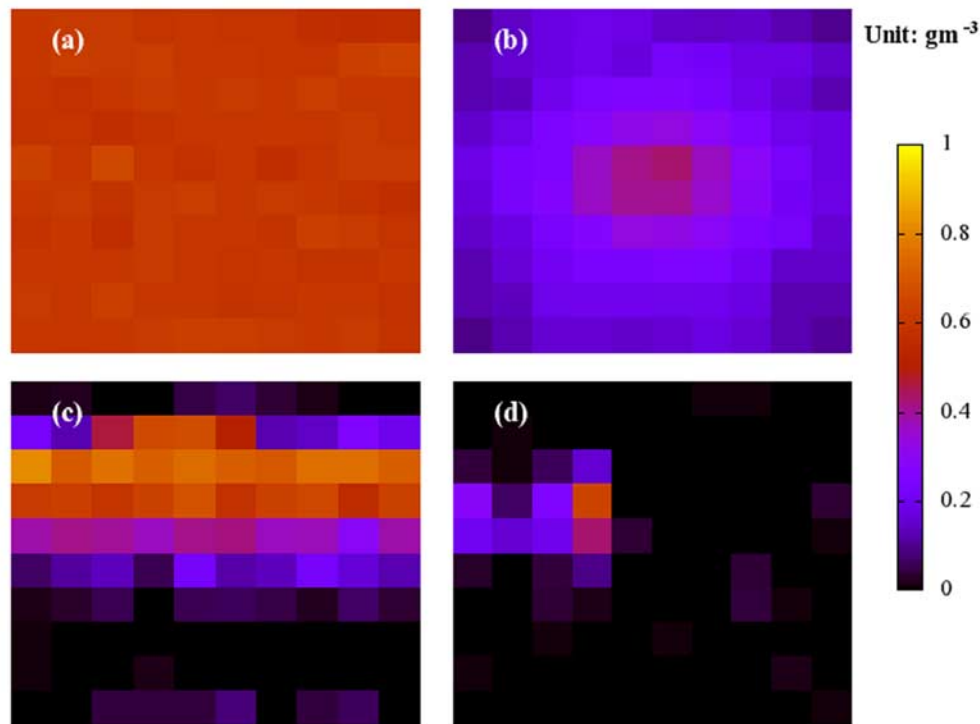


Figure 6. Retrieved liquid water fields for the aforementioned cloud cases using cloud tomography setup III (four radiometers of 0.3 K noise level, 200 scanning angles, 10 by 10 output resolution): (a) homogeneous cloud, (b) onion cloud, (c) stratocumulus cloud, and (d) broken cumulus cloud.

method for each combination of cloud case/tomography setup is shown in Table 1. The retrieval error from Warner’s dual-radiometer setup is more than 10% for the first three cloud cases at 10 by 10 output resolution. With four-radiometer, the cloud tomography method can retrieve LWC within 5% accuracy at the same spatial resolution. The eight-radiometer setup further improves the retrieval to an accuracy of about 3% at 10 by 10 resolution. However, the retrieval accuracy with the eight-radiometer setup degrades to about 6% at 20 by 20 resolution. These results indicate that adding more radiometers tends to improve the tomographic retrieval, while increasing output resolution leads to the opposite direction.

[26] The metric for the standard least squares method is shown in Table 1 in the parenthesis. The error of the standard least squares method is always higher than that of the truncated SVD method. For Setup I the error of the standard least squares method is about 2.8 times as that of the truncated SVD, for Setup II the ratio is 2.6, for Setup III the ratio is 1.7, and for Setup IV the ratio is 4.0. Such large discrepancies suggest that the truncated SVD method is superior to the standard method in obtaining more accurate retrieval especially when only a few radiometers are used or a high output resolution is required.

[27] Figure 6 shows the retrieved fields of the four cloud cases for Setup III (4 radiometers, 10 by 10 output resolution). In all examples, the reconstructed images well capture the spatial patterns of LWC in the original images. For the homogeneous cloud case, the retrieval successfully reproduces the homogeneous field. The juicy core in the onion cloud case is correctly located in the reconstructed image.

The horizontal homogeneity and vertical heterogeneity in the stratocumulus cloud case are reasonably captured by the retrieval. The retrieval also reproduces the location and extent of each cloud patch in the broken cloud case. Figure 7 shows the corresponding retrieval error fields for each case, calculated as the absolute difference between the true and retrieved fields. There are no clear spatial patterns in the retrieval error fields. Overall, the spatial patterns of LWC are well reproduced in the tomographic retrievals.

[28] An important cloud property of interest to the climate modelers is the Liquid Water Path (LWP), the vertically integrated LWC. Figure 8 suggests that the retrieved LWP compares favorably with the true LWP in 10 vertical columns of the clouds. The maximum error is approximately 20 gm^{-2} , which is similar to that of the zenith-looking MicroWave Radiometer (MWR) at the ARM sites [Liljegren *et al.*, 2001]. An apparent advantage of cloud tomography over the MWR is that LWP over multiple locations can be measured simultaneously without moving the radiometers to all these locations.

4.2. Sensitivity Studies

[29] The accuracy of the cloud tomography retrievals depends on many factors. Among these are the number of radiometers, the output resolution, the number of scanning directions, the receiver noise level, the antenna beam width, and the uncertainty of the required ancillary data such as the atmospheric temperature and water vapor mixing ratio. This section examines the impacts of these factors on the retrieval quality. The third cloud case (stratocumulus) is used in the sensitivity studies.

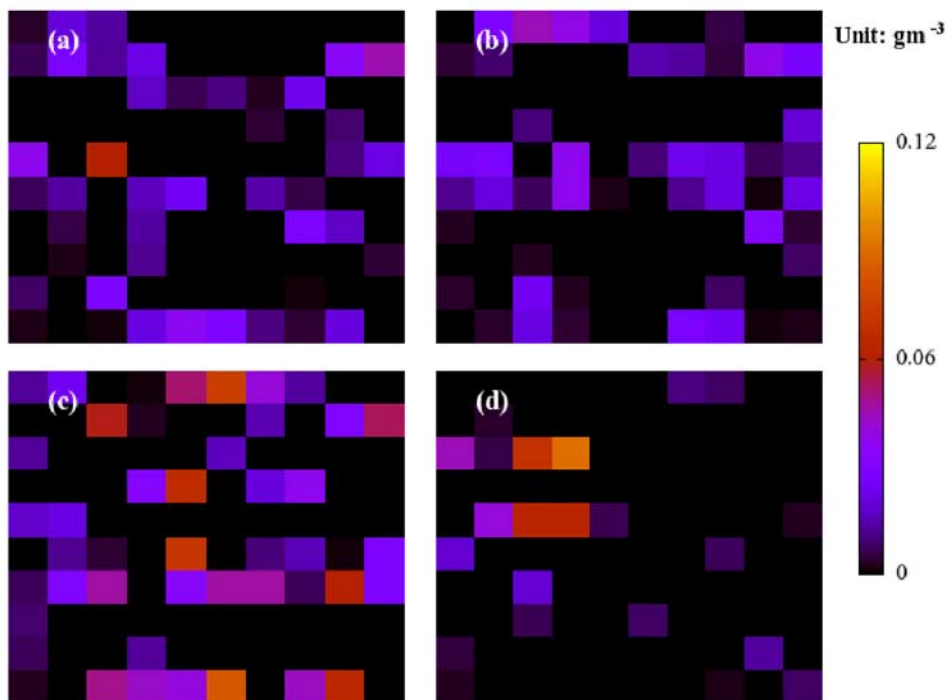


Figure 7. Retrieval error fields calculated as the absolute difference between Figures 5 and 6: (a) homogeneous cloud, (b) onion cloud, (c) stratocumulus cloud, and (d) broken cumulus cloud.

4.2.1. Number of Radiometers and Output Resolution

[30] The first factor investigated is the number of radiometers. Figure 9a depicts the representative decreasing trend of the retrieval error with the number of radiometers. With few radiometers, say two, adding one more improves the retrieval significantly. Warner’s dual-radiometer setup is indicated by a dash-dotted line; it is clearly not optimal for retrieving the stratocumulus cloud at 10 by 10 resolution. When there are already four radiometers, including an additional one doesn’t yield significant improvement. This suggests that the optimal number of radiometers is four when the desired output resolution is a few hundred meters. Our simulations show that this result is also valid for the other cloud cases. The dashed curve in Figure 9a shows that the condition number shares the same trend as the retrieval error. Recall that a higher condition number usually means the underlying problem is more ill-posed and thus a larger retrieval error is more likely. Retrieval becomes less ill-posed when more radiometers are used, which is consistent with the trend of retrieval error.

[31] The next factor examined is the output resolution. Output resolution determines the finest spatial scale to be resolved. Figure 9b reveals that forcing cloud tomography to retrieve finer structure results in an increased error in the retrieval. A close inspection of Figure 9b suggests that, at very coarse resolution, the retrieval problem is not ill-posed (characterized by a small condition number) and thus the retrieval error is very small. The ill-posedness of the retrieval problem keeps increasing at the region of intermediate resolution, which results in a rapid increase in the retrieval error at this region. The increase of the retrieval error becomes less rapid, though the condition number keep increasing with the output resolution after the point of 24 by

24. The reason for this is that the retrieval problem has already been very ill-posed and the best retrieval has been achieved with a big truncating parameter, in other words, the retrieved cloud field has been constrained to be almost homogeneous and hence the retrieval is almost nothing but a regularization artifact. The high condition number and the resultant large retrieval errors at a high output resolution indicate that more radiometers and/or radiometers with lower noise level are needed to retrieve cloud information at such a fine scale.

[32] The number of radiometers sets a physical limit on the smallest spatial scale to which the cloud tomography method can resolve. For a given number of radiometers, the choice of output resolution should be based on the desired retrieval accuracy.

4.2.2. Number of Scanning Angles and Radiometer Noise Level

[33] Figure 10a suggests that the retrieval is more accurate when each cloud pixel is viewed from more directions. The condition number shares the same trend; it means the retrieval problem becomes less ill-posed with increasing number of scanning angles. In addition, Figure 10a indicates that beyond some point, say three scanning angles per pixel, increasing the number of scanning angles is no longer a good strategy to improve the retrieval - both the retrieval error and the condition number level off.

[34] The next factor examined is the radiometer noise level. Figure 10b shows that the retrieval error increases with the radiometer noise level, as one would expect. When the microwave signal is free of noise, cloud tomography reconstructs the cloud field exactly. The retrieval error first increases fast when the noise level is very low and then becomes less sensitive when the noise level is very high,

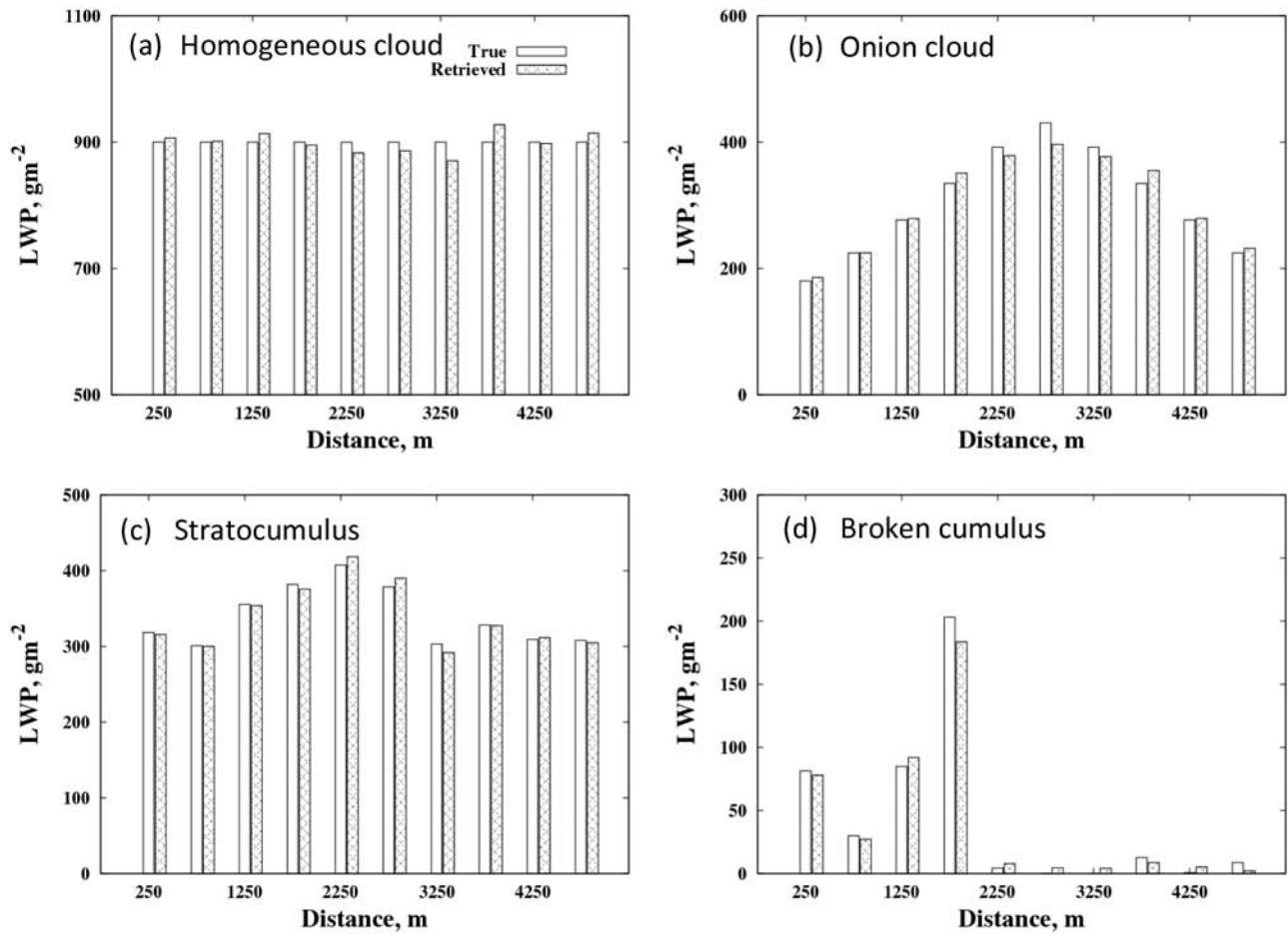


Figure 8. Comparison of the true LWP as a function of location with the LWP computed from the liquid water fields retrieved with the tomography setup III for the following cloud cases: (a) homogeneous cloud, (b) onion cloud, (c) stratocumulus cloud, and (d) broken cumulus cloud.

while the condition number shows no variation. Since the condition number is a characteristic of only the matrix \mathbf{A} (see equation (4), \mathbf{A} is weakly depended on the transmission terms in equation (5) therefore is a weak function of cloud

liquid water), it is not surprising that the condition number does not change with the noise level at all (Figure 10b). Therefore condition number can be viewed as an intrinsic characteristic of the tomography setup.

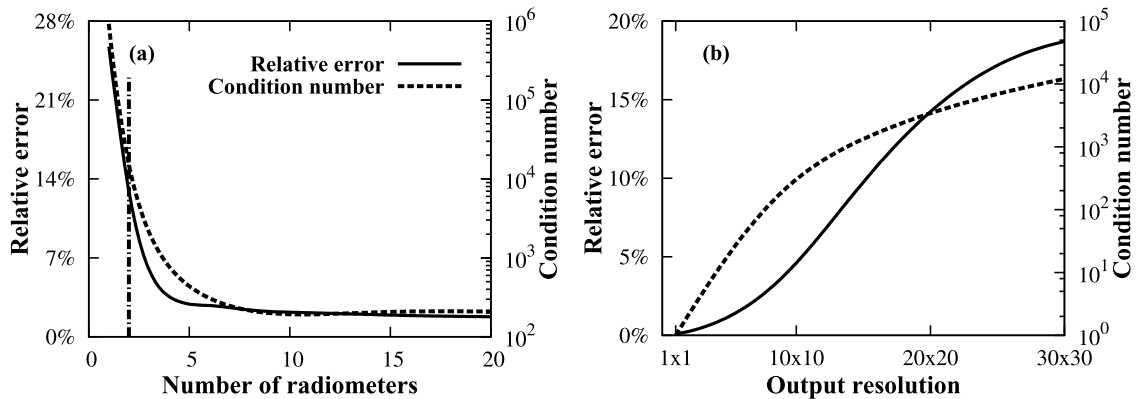


Figure 9. Impacts of the number of radiometers and the output resolution on the tomographic retrievals. The LES stratocumulus cloud is used for this sensitivity test. The relative retrieval error, as well as the corresponding condition number, decreases when: (a) more radiometers are used, and/or (b) a coarser output resolution is chosen. Warner’s dual-radiometer setup is indicated by a vertical dash-dotted line in (Figure 9a). Apparently, it is not the optimal choice for this case.

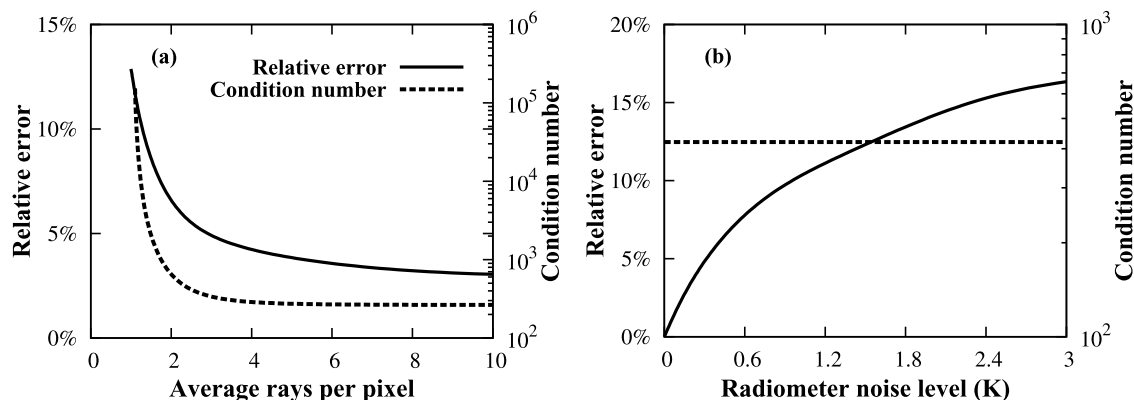


Figure 10. Impacts of the average number of rays per pixel and the radiometer noise level on the tomographic retrievals. The LES stratocumulus cloud is used for this sensitivity test. The relative retrieval error decreases with: (a) increasing number of scanning angles per pixel, and/or (b) decreasing radiometer noise level. The corresponding condition number also decreases with increasing rays per pixel, but remains unchanged with changing radiometer noise level.

[35] It is worth to mention that, operationally, the radiometer noise level trades off against the number of scanning angles because more scan angles means shorter dwell time for each measurement and thus larger noise. The optimal choice of these parameters can be figured out by a similar analysis as presented in Figures 10a and 10b.

4.2.3. Antenna Beam Width

[36] Antenna beam width is an important characteristic of microwave radiometers and is expected to affect the tomographic retrieval. Figure 11 shows that the relative retrieval error and the corresponding condition number increase with the beam width. This suggests that a broader beam width provides less information about cloud structure if other specifications remain the same. Nevertheless, the typical beam width of operational microwave radiometers nowadays ranges from 1° to 8° , only leading to a minor difference in the tomographic retrieval.

4.2.4. Physical Arrangement of Radiometers

[37] Our default setup assumes the radiometers are equally arranged on a line of 10 Km. Here we keep the linear arrangement but vary the separation between radiometers, i.e., the distance between the first and last radiometers on the line. Figure 12 shows the variation of the retrieval error and the corresponding condition number as a function of the radiometer separation for three tomographic setups (four-radiometer, eight-radiometer, and sixteen-radiometer). At the zero separation (putting the radiometers at the same ground location), which essentially forces the radiometers to work like one radiometer, the retrieval error is very large (more than 80%, not shown in Figure 12). The retrieval error decreases as the separation is increased up to 4 Km for all of the three setups (Figure 12a), which indicates that moving the radiometers apart adds more useful information about cloud structure to the measurements. This is also confirmed by the trend of the condition number (Figure 12b). For the four-radiometer setup, the retrieval error starts to increase with further increasing distance (the same trend is more evident for the condition number), suggesting that 4 Km is about the optimal separation. For the eight-radiometer setup, the retrieval error remains flat with further increasing radiometer separation and then increases slowly when

the separation is larger than 12 km (better illustrated by the condition number in Figure 12b). For the sixteen-radiometer setup, the retrieval error and the condition number remain flat or decrease very slowly with increasing separation.

[38] The different behaviors of the retrieval error as a function of the radiometer separation for the three setups can be explained as the trade-off between two competing requirements: the need for continuously angular samples, and the need for sampling a large range of angles for each cloud pixel. The first need requires the radiometers to space as close to each other as possible, while the second one prefers the radiometers to span a distance as large as possible.

4.2.5. Uncertainty in Environment Temperature and Water Vapor Mixing Ratio

[39] Some ancillary data such as environment temperature and water vapor mixing ratio are necessary to calculate the absorption coefficient of liquid water and the microwave contribution from water vapor emission. Such data can be

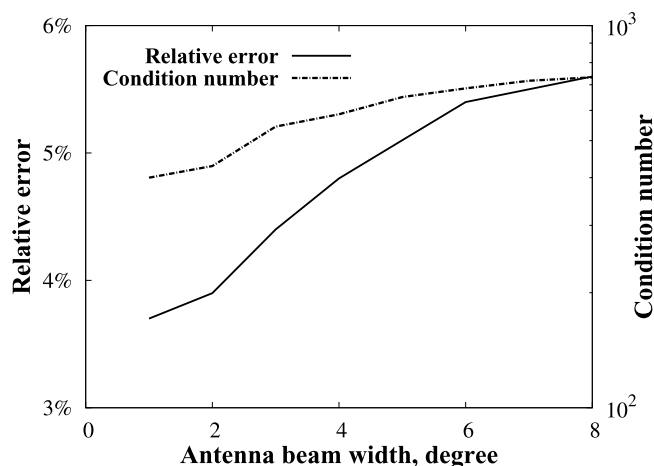


Figure 11. Relative retrieval error and the corresponding condition number increase with increasing antenna beam width. The LES stratocumulus cloud is used for this sensitivity test.

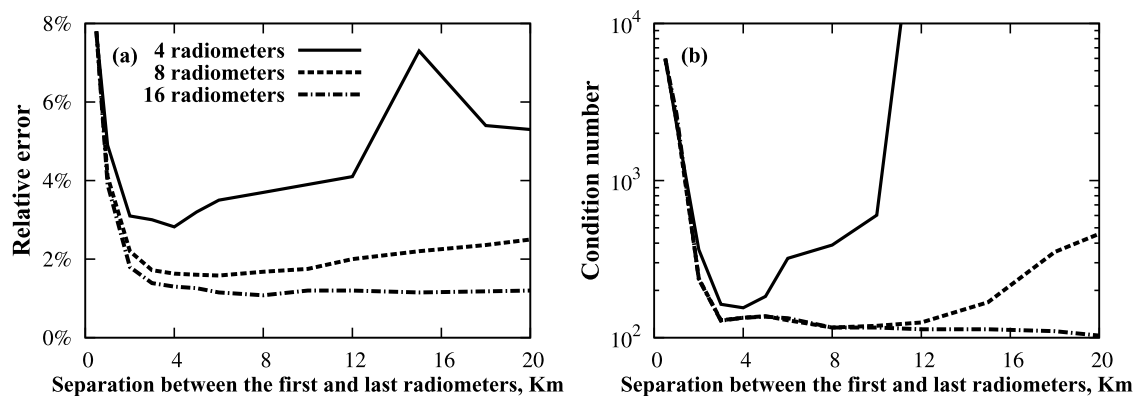


Figure 12. Impact of the physical arrangement of radiometers on the tomographic retrievals. (a) The relative retrieval error and (b) the corresponding condition number are shown as a function of the separation between the first and last radiometers. The LES stratocumulus cloud is used for this sensitivity test. Three setups with four, eight, and sixteen radiometers are examined. For the four-radiometer setup, the optimal distance is around 4 km. For the other two setups, the optimal distance is not so clear and lies in a much larger range, say 4–12 km.

acquired using a meteorological radiosonde or aircraft sounding. The uncertainty of these data of course should have an impact on the tomographic retrieval. Figure 13 shows that the relative retrieval error changes with various degrees of uncertainty in the temperature and water vapor mixing ratio data. The retrieval error increases with increasing uncertainty in the input temperature and water vapor data, but the range of the retrieval error is small at even relatively large uncertainty levels of the ancillary data. This confirms the statement by Warner *et al.* [1985], “the accuracy within which these quantities needs to be known is not very high, being well within the limits which would be available from a nearby radiosonde or research aircraft sounding”. The relatively low sensitivity to temperature and water vapor, however, prevents from retrieving these two quantities using the 31 G frequency. It would be possible to retrieve them if other appropriate frequencies are included.

[40] In summary, the retrieval accuracy of cloud tomography is mainly determined by the characteristics (such as noise level and beam width) and the physical arrangement

of radiometers, the radiometer scanning strategy, and the uncertainty in the ancillary data.

5. Concluding Remarks and Discussions

[41] The cloud tomography method has been revisited and extended, with emphasis on understanding the mathematical nature of the retrieval problem and its relationship to the physical configuration of the cloud tomography system. The retrieval problem is found to be highly ill-posed, and as a result, the standard least squares method fails to produce the optimal retrieval. Instead, the truncated SVD method is successfully used in the retrieval algorithm, and it produces more accurate retrievals than the standard method. A group of sensitivity simulations show that the retrieval of cloud LWC depends on the radiometer noise level, the antenna beam width, the total number of scanning angles, the number of radiometers, the output resolution, the physical arrangement of radiometers, and the uncertainty in the input ancillary data (environment temperature and water vapor mixing ratio). When more radiometers and/or more scan-

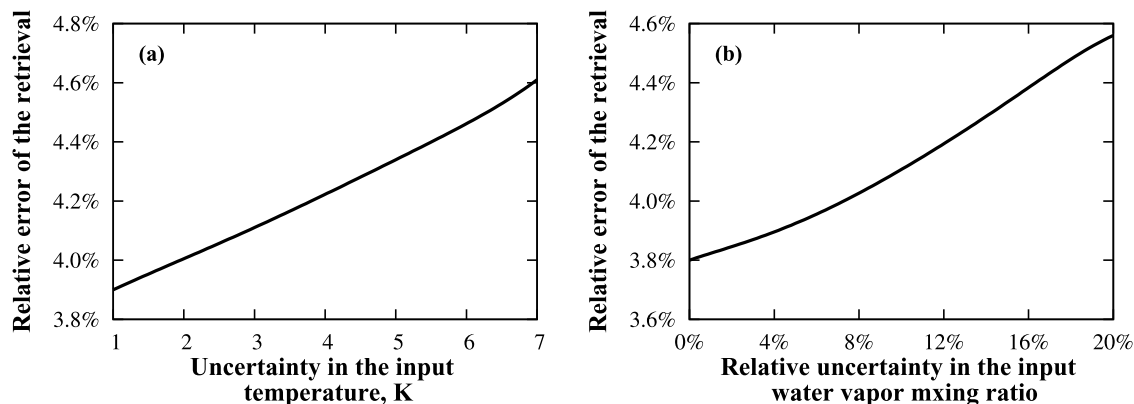


Figure 13. Relative retrieval error as a function of the uncertainty in the ancillary data: (a) atmospheric temperature, and (b) water vapor mixing ratio. The LES stratocumulus cloud is used for this sensitivity test. These results show that, when measuring a moderately thick cloud using the cloud tomography method, the requirement for accuracy of water vapor and environment temperature to be known is not high.

ning angles are used, and/or the radiometer beam width is reduced, and/or when a coarser output resolution is acceptable, the retrieval problem becomes less ill-posed, and a better retrieval can be obtained. The uncertainty in the ancillary data such as environment temperature and water vapor mixing ratio also impacts the retrieval, but the impact is considerably small over the range of uncertainty levels provided by radiosonde or sounding measurements. Moreover, modern cloud-resolving models allow us to examine the capability of cloud tomography to retrieve more realistic cloud structure. With a cloud tomography setup consisting of four radiometers of 0.3 K noise level, the RMS errors of the reconstructed LWC images are within 5% of the maximum values of LWC present in the clouds. Overall, the application of the cloud tomography method will add a great deal information to existing cloud measurements at a relatively modest cost compared to scanning radar.

[42] The retrieval algorithms of limited angle tomography usually make use of some prior knowledge to reduce variability in the retrieval and improve the reconstructed image [Rangayyan *et al.*, 1985]. In this work, smoothness constraint has been employed in our retrieval algorithm through the so-called truncated SVD method. Similarly, a nonnegative constraint can be imposed to further reduce the function space of retrieval, and this additional constraint is likely to improve the retrieval of small LWCs [Liu *et al.*, 1999]. Another potentially useful constraint is the adiabatic LWC, which provides an upper bound for the retrieval. Other measurements such as from a cloud radar or infrared thermometer can also serve as further constraints to improve the tomographic retrieval. We plan to examine these issues in the future studies.

[43] Microwave emission from cloud liquid water is assumed to be proportional to liquid water mass and independent of other moments of the droplet size distribution, as was mentioned earlier in this paper. This assumption would be violated if a substantial number of large drops (e.g., drizzle or raindrop) are present in clouds so that the underlying Rayleigh approximation is no longer valid at the 31 GHz frequency. Appropriate correction should be included if the cloud tomography method is used to retrieve precipitating clouds. Also the presence of ice crystals in clouds would complicate cloud tomography because they are good scatterers at the microwave region. These issues will be investigated in our future studies.

[44] **Acknowledgments.** This research is supported by the DOE Atmosphere Radiation Measurement program under Contract DE-AC02-98CH10886. It is a pleasure to acknowledge the insightful discussions with Kollias Pavlos, Andy Volgemann, Mark Miller, and Richard Cederwall. The authors also thank Ed Westwater for providing the photograph of the microwave radiometers. We are also thankful to the anonymous reviewers whose stimulating comments greatly helped to improve this paper.

References

- Ackerman, T., and G. Stokes (2003), The atmospheric radiation measurement program, *Phys. Today*, *56*, 38–45.
- Ackerman, S. A., O. B. Toon, and P. V. Hobbs (1995), A model for particle microphysics, turbulent mixing, and radiative transfer in the stratocumulus topped marine boundary layer and comparisons with measurements, *J. Atmos. Sci.*, *52*, 1204–1236.
- Cimini, D., E. R. Westwater, A. J. Gasiewski, M. Klein, V. Y. Leuski, and S. G. Dowlatshahi (2007), The ground-based scanning radiometer: A powerful tool for study of the Arctic atmosphere, *IEEE Trans. Geosci. Remote Sens.*, *45*, 2759–2777.
- Davison, M. E. (1983), The ill-conditioned nature of the limited angle tomography problem, *SIAM J. Appl. Math.*, *43*(2), 428–448.
- Drake, J. F., and J. Warner (1988), A theoretical study of the accuracy of tomographic retrieval of cloud liquid with an airborne radiometer, *J. Atmos. Sci. Oceanic Technol.*, *5*, 844–857.
- Falcone, V. (1966), Calculation of apparent sky temperature at millimeter wavelengths, *Radio Sci.*, *1*(new series), 1205–1209.
- Fleming, H. E. (1982), Satellite remote sensing by the technique of computed tomography, *J. Appl. Meteorol.*, *21*, 1538–1549.
- Flores, A., G. Ruffini, and A. Rius (2000), 4D tropospheric tomography using GPS slant wet delays, *Ann. Geophys.*, *18*, 223–234.
- Hansen, P. C. (1990), Truncated singular value decomposition solutions to discrete ill-posed problems with ill-determined numerical rank, *SIAM J. Sci. Stat. Comput.*, *11*, 503–518.
- Hansen, P. C. (1992), Analysis of discrete ill-posed problems by means of the L-curve, *SIAM Rev.*, *34*, 561–580.
- Hansen, P. C. (1998), *Rank Deficient and Ill-posed Problems: Numerical Aspects of Linear Inversion*, p. 247, SIAM, Philadelphia, PA.
- Hoffman, R. N., C. Grassotti, R. G. Isaacs, and T. J. Kleespies (1989), A simulation study of satellite emission computed tomography, *J. Appl. Meteorol.*, *28*, 321–342.
- Hogan, R. J., N. Gaussiat, and A. J. Illingworth (2005), Stratocumulus liquid water content from dual-wavelength radar, *J. Atmos. Oceanic Technol.*, *22*, 1207–1218.
- Hogg, D. C., F. O. Guiraud, J. B. Snider, M. T. Decker, and E. R. Westwater (1983), A steerable dual-channel microwave radiometer for measurement of water vapor and liquid in the troposphere, *J. Appl. Meteorol.*, *22*, 789–806.
- Lawson, C. L. and R. J. Hanson (1974), *Solving Least Squares Problems*, pp. 158–169, Prentice-Hall, Englewood Cliffs, N. J.
- Liljegren, J., E. Clothiaux, G. Mace, S. Kato, and X. Dong (2001), A new retrieval for cloud liquid water path using a ground-based microwave radiometer and measurements of cloud temperature, *J. Geophys. Res.*, *106*, 14,485–14,500.
- Liu, Y., W. P. Arnott, and J. Hallett (1999), Particle size distribution retrieval from multispectral optical depth: Influences of particle nonsphericity and refractive index, *J. Geophys. Res.*, *104*, 31,762.
- Mattioli, A., E. R. Westwater, S. I. Gutman, and V. R. Morris (2005), Forward model studies of water vapor using scanning microwave radiometers, global positioning system, and radiosondes during the cloudiness intercomparison experiment, *IEEE Trans. Geosci. Remote Sens.*, *43*, 1012–1023.
- Olson, T. (1995), A stabilized inversion for limited angle tomography, *IEEE Biomed. Eng.*, *14*, 612–620.
- Rangayyan, R., A. P. Dhawan, and R. Gordon (1985), Algorithms for limited view computed tomography - An annotated bibliography and a challenge, *Appl. Opt.*, *24*, 4000–4012.
- Snider, J. B., H. M. Burdick, and D. C. Hogg (1980), Cloud liquid measurement with a ground-based microwave instrument, *Radio Sci.*, *15*, 69–683.
- Stephens, G. L. (2005), Cloud feedbacks in the climate system: A critical review, *J. Climate*, *18*, 237–273.
- Twomey, S. (1987), Iterative nonlinear inversion methods for tomographic problems, *J. Atmos. Sci.*, *44*, 3544–3551.
- Warner, J., and J. F. Drake (1988), Field tests of an airborne remote sensing technique for measuring the distribution of liquid water in convective cloud, *J. Atmos. Oceanic Technol.*, *5*, 833–843.
- Warner, J., J. F. Drake, and P. R. Krehbiel (1985), Determination of cloud liquid water distribution by inversion of radiometric data, *J. Atmos. Sci. Oceanic Technol.*, *2*, 293–303.
- Warner, J., J. F. Drake, and J. B. Snider (1986), Liquid water distribution obtained from coplanar scanning radiometers, *J. Atmos. Sci. Oceanic Technol.*, *3*, 542–546.
- Westwater, E. R. (1972), Microwave emission from clouds, NOAA Tech. Rep. ERL 219-WPL, 18, p. 43.
- Westwater, E. R., S. Crewell, and C. Matzler (2004), A review of surface based microwave and millimeter wave radiometric remote sensing of the troposphere, *Radio Sci. Bull.*, *3010*, 59–80.
- Wiscombe, W. J. (2005), Scales, tools, and reminiscences, in *Three-Dimensional Radiative Transfer in the Cloudy Atmosphere*, edited by A. Marshak and A. B. Davis, pp. 3–92, Springer, New York.

D. Huang, Y. Liu, and W. Wiscombe, Environmental Sciences Department, Brookhaven National Laboratory, 75 Rutherford Drive, Upton, NY 11973, USA. (dhuang@bnl.gov)